Origin of nanomechanical cantilever motion generated from biomolecular interactions

Guanghua Wu*, Haifeng Ji†, Karolyn Hansen†, Thomas Thundat†, Ram Datar‡, Richard Cote‡, Michael F. Hagan§, Arup K. Chakraborty§, and Arunava Majumdar*¶

*Department of Mechanical Engineering, University of California, Berkeley, CA 94720; †Life Sciences Division, Oak Ridge National Laboratory, Oak Ridge, TN 37831; ‡Department of Pathology, University of Southern California, Los Angeles, CA 90033; and §Departments of Chemical Engineering and Chemistry, Materials Science Division, Lawrence Berkeley National Laboratory, University of California, Berkeley, CA 94720

Edited by Calvin F. Quate, Stanford University, Stanford, CA, and approved November 27, 2000 (received for review August 1, 2000)

Generation of nanomechanical cantilever motion from biomolecular interactions can have wide applications, ranging from high-throughput biomolecular detection to bioactuation. Although it has been suggested that such motion is caused by changes in surface stress of a cantilever beam, the origin of the surface-stress change has so far not been elucidated. By using DNA hybridization experiments, we show that the origin of motion lies in the interplay between changes in configurational entropy and intermolecular energetics induced by specific biomolecular interactions. By controlling entropy change during DNA hybridization, the direction of cantilever motion can be manipulated. These thermodynamic principles were also used to explain the origin of motion generated from protein–ligand binding.

Understanding the mechanisms of how biological reactions produce motion is fundamental to several physiological processes (1–3). Although most past effort (4–6) has focused on studying single molecular motors (7–9), recent experiments (10, 11) by using microcantilever beams have led to observations that multiple DNA hybridization and antigen–antibody reactions can collectively produce nanomechanical motion. The promising prospects of interfacing molecular biology with micro- and nanomechanical systems can best be exploited if we learn how to control and manipulate nanomechanical motion generated by biomolecular interactions. Although an understanding of the origins of this motion would allow such control, it has so far remained elusive. It has been suggested (11) that the motion is induced by changes in surface stress of the cantilever caused by biomolecular binding. Although this may be true, the origin of surface-stress change is not understood. In this paper, we show that cantilever motion is created because of the interplay between changes in configurational entropy and intermolecular energetics induced by specific biomolecular reactions. The entropy contribution can be critical in determining the direction of motion. By using thermodynamic principles in conjunction with DNA hybridization experiments, we demonstrate that both the direction and magnitude of cantilever motion can be controlled. These thermodynamic principles are also used to explain the nanomechanical motion created by protein–ligand binding.

Materials and Methods

Experimental Setup and Approach. Fig. 1 illustrates the experiment we used for studying nanomechanical motion created by multiple specific biomolecular reactions. The experimental setup consisted of a transparent fluid cell, within which a gold-coated silicon nitride (Au/SiN_x) cantilever was mounted. The fluid cell and the V-shaped micromechanical silicon nitride cantilevers were purchased from Digital Instruments (Santa Barbara, CA). The cantilevers used were 200 μm long and 0.5 μm thick, and each leg was 20 μm wide. The gold films originally coated on cantilevers were etched away, and a fresh 25-nm-thick gold coating was deposited. For good adhesion between gold and silicon nitride, a 5-nm-thick chrome film was deposited on the nitride cantilever before the gold deposition. When the fluid cell was clamped down on a glass slide with a Teflon O-ring, the cell formed a liquid reservoir about 100 μl in volume that was connected to an inlet and an outlet fluid port. To detect cantilever deflections, a low-power ($\approx$1-mW) laser beam was reflected off the cantilever and was focused onto a position-sensitive detector. Such a setup is commonly used in atomic force microscopes. To eliminate thermomechanical motion of the Au-SiN_x bimaterial cantilever caused by temperature fluctuations, the glass slide and fluid cell were mounted on thermoelectric coolers so that the temperature of the fluid cell could be controlled to 25 $\pm$ 0.05°C.

The experiment started by first placing a Au/SiN_x cantilever in a fluid cell and then injecting a solution of sodium phosphate buffer (PB) at pH $\approx$7.0 (always with the same pH but possibly different ion concentrations for different experiments) into the cell. The cantilever was equilibrated in the PB until a stable baseline was obtained. The next step was to immobilize the probe molecules, which were resuspended in the same PB used to equilibrate the cantilever, on the cantilever surface. After the immobilization was completed (typically about 2 hours at room temperature), the fluid cell was washed thoroughly with the PB to be used for hybridization. Then the cantilever was equilibrated in the same PB (as that to be used for hybridization) again until a stable baseline was obtained. Finally, injection of a solution of target molecules (resuspended in the same PB) followed. The cantilever motion was optically monitored at both the immobilization and probe-target-binding steps. For each experiment, a new cantilever was used. The error induced by variations in the geometry of the cantilever (length, width, and thickness) and the position of the focused laser spot at the end of the cantilever was found to be within $\pm$5–10%. To address the effect of change in the refractive index, experiments in which the laser was focused on the cantilever substrate were carried out. When the ion concentration of PB was changed from 0.05 to 1.0 M, no significant change in the position-sensitive detector signal was observed, which indicates that the effect of change in the refractive index is negligible for our experiments.

DNA Samples. All single-stranded DNA (ssDNA) samples were bought from Synthegen (Houston, TX). To form a self-assembled monolayer of probe ssDNA on the Au-coated cantilever surface, the ssDNA was modified with thiol groups attached to the 5′ end. The thiol groups used for immobilizing probe ssDNA were HS-$(CH_2)_6$ and were always attached to the

This paper was submitted directly (Track II) to the PNAS office.

Abbreviation: ssDNA, single-stranded DNA.

¶To whom reprint requests should be addressed. E-mail: majumdar@me.berkeley.edu.

The publication costs of this article were defrayed in part by page charge payment. This article must therefore be hereby marked "*advertisement*" in accordance with 18 U.S.C. §1734 solely to indicate this fact.

Article published online before print: *Proc. Natl. Acad. Sci. USA*, 10.1073/pnas.031362498. Article and publication date are at www.pnas.org/cgi/doi/10.1073/pnas.031362498

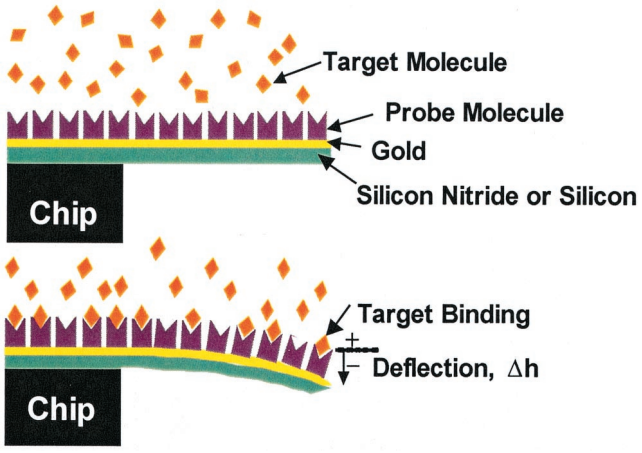

Fig. 1. Specific biomolecular interactions between target and probe molecules alter intermolecular interactions within a self-assembled monolayer on one side of a cantilever beam. This can produce a sufficiently large force to bend the cantilever beam and generate motion. The origin of this nanomechanical motion lies in the interplay between changes in configurational entropy and intermolecular energetics.

5′ end of the ssDNA. For the experiments discussed in Fig. 2*a*, the 50-nt-long (sequence J) probe ssDNA sequences used were 5′-TTGCTCTGCACCGACAATTTAGCGCCAGCTTACTG-CTGGAATCGGTTCTG-3′ (3.2 μM, 50 ng/μl). The sequence for the 40-nt-long ssDNA (sequence K-40) used for the data in the Fig. 2 *Inset* was 5′-TTAAGGTCTGGACTGGCCTGAATT-TAGCGCCAGCTTACTG-3′ (3.2 μM, 40 ng/μl). The sequences for 30-nt-long (sequence K-30: 5′-TTAAGGTCTG-GACTGGCCTGAATTTAGCGC-3′, 3.2 μM, 30 ng/μl) and 20-nt-long (sequence K-20: 5′-TTAAGGTCTGGACTGGC-CTG-3′, 3.2 μM, 20 ng/μl) ssDNA used for the Fig. 2*a Inset* were the first 30 and first 20 nucleotide sequences from sequence K-40, starting from the 5′ end (see below). Sequence K-30 was used for the data in Fig. 2*b*. For the data in Fig. 3*a*, the 20-nt-long probe ssDNA used was sequence K-20. The complementary target ssDNA sequences were 3′-AATTCCAGACCTGACCG-GAC-5′ (20 nt long, 6.4 μM, 40 ng/μl), 3′-CAGACCTGAC-CGGAC-5′ (15 nt long, 6.4 μM, 30 ng/μl), 3′-CTGACCG-GAC-5′ (10 nt long, 6.4 μM, 20 ng/μl), and 3′-TGACCGGAC-5′ (9 nt long, 6.4 μM, 18 ng/μl). The noncomplementary sequence (sequence-NC20) used was 3′-CTATGACAGATCTACTCGTA-5′ (6.4 μM, 40 ng/μl). In all of the hybridization experiments, the concentration of thiolated probe ssDNA was 50 ng/μl (8 μM). For Fig. 3*b*, sequence K-30 was used as the probe ssDNA, and the target ssDNA was sequence K′-30 (3′-AATTCCAGACCTGACCGGACTTA-AATCGCG-5′, 3.2 μM, 30 ng/μl). For Fig. 5, sequence K-30 was used as probe ssDNA, and K′-30 was used as the target ssDNA.

Biotin–Neutravidin Experiments. Biotinylation of Au/SiN_x cantilevers was accomplished by first functionalizing the SiN_x surface with a 1% solution (volume to volume) of 3-aminopropyl triethoxysilane (Gelest, Tullytown, PA) in absolute ethanol for 1 h. Aminosilane surfaces were subsequently functionalized with 1 mM NHS-PEG-Biotin, MW 3400 (PEG, polyethylene glycol; Shearwater Polymers, Huntsville, AL) in PBS (pH 7.5, 10 mM phosphate/150 mM saline) for 1 h. Cantilevers were rinsed extensively in PBS; all binding experiments were carried out under flow (4 ml/hr) in PBS. Neutravidin, MW 60 K_d (Pierce, Rockford, IL), 25 ng/μl, was injected in-line by using injection loops (Upchurch Scientific, Oak Harbor, WA). Silanized cantilever was exposed to 500-μl injection (12.5 μg of neutravidin), and PEG–biotin cantilever was exposed to 20-μl injection (500 ng of neutravidin).

Results and Discussion

Fig. 2*a* shows the cantilever deflection as a function of time for a 50-nt-long probe ssDNA. Here, negative deflection indicates the downward bending of the cantilever with the probe molecules immobilized on the top surface. Also shown are the deflection profiles after the injection of PB alone and of unthiolated ssDNA, which represent the control experiments. The injection of PB alone produces almost no change in deflection, and the injection of unthiolated ssDNA produces very small

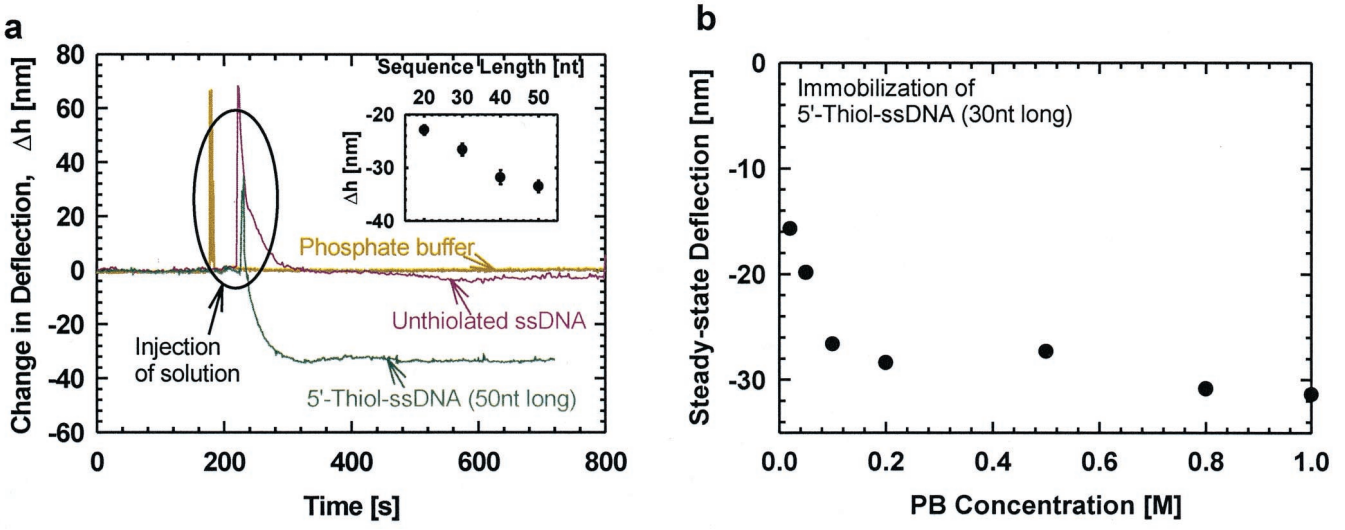

Fig. 2. (*a*) Change in Au/SiN_x cantilever deflection as a function of time for three different experiments: (*i*) exposure to 0.1 M PB; (*ii*) exposure to unthiolated probe ssDNA; (*iii*) exposure to probe ssDNA thiolated at the 5′ end. Concentrations of unthiolated and single-end thiolated ssDNAs were all 50 ng/μl or approximately 3.2 μM. Unthiolated ssDNA and pure PB solutions did not produce any significant deflection. *Inset* shows the steady-state cantilever deflection as a function of length of the probe ssDNA thiolated. Results indicate that immobilization of probe ssDNA produces compressive stress bending the cantilever down. (*b*) Steady-state cantilever deflections caused by immobilization of ssDNA (sequence K-30) at different PB concentrations.

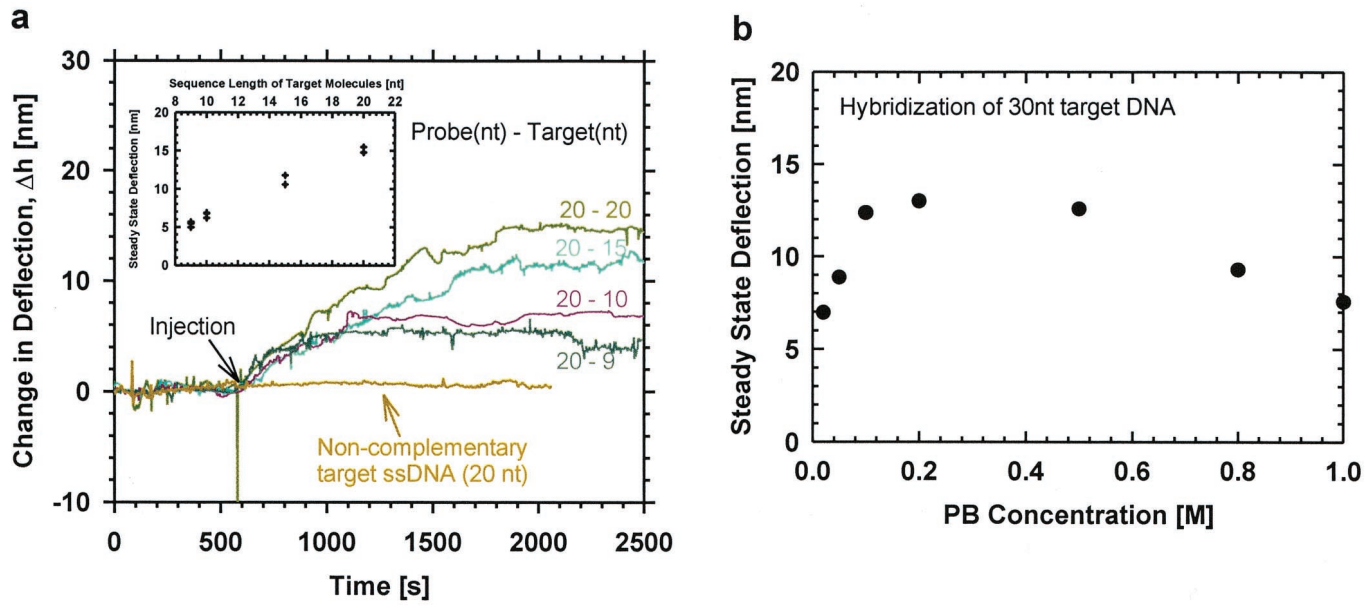

Fig. 3. (*a*) Changes in Au-Si cantilever deflection caused by hybridization of a probe ssDNA (sequence K-20 at 50 ng/μl or 8 μM concentration) in the distal end with complementary target ssDNA of different lengths—20 nt, 15 nt, 10 nt, and 9 nt (40 ng/μl or 3- to 6-μM concentration). Also shown is the absence of cantilever deflection for a noncomplementary target ssDNA (sequence NC20). The data clearly suggest that differences in nanomechanical motion caused by a 1-nt difference in length can be observed. (*b*) Steady-state changes in cantilever deflection for hybridization of 30-nt-long ssDNA (sequences K-30 and K′-30) at different PB concentrations. Note that immobilization of probe ssDNA (sequence K-30) were at the same PB concentration (0.1 M) as the hybridization reaction for both *a* and *b*.

downward deflection because of nonspecific binding of ssDNA to the gold surface. Fig. 2*a Inset* shows the steady-state cantilever deflection as a function of the length of the probe ssDNA. Fig. 2*b* shows the cantilever deflection as a function of PB concentration after immobilizing 30-nt-long probe ssDNA. The concentration used for all probe ssDNAs was 3.2 μM. Surface plasmon resonance spectroscopy measurements (14, 15) have shown that under conditions similar to our experiments, the surface density of thiol-tethered ssDNA on the gold surface is around 6×10^{12} chains/cm^2. It is clear from these experiments that regardless of the length of ssDNA or ionic strength used in the experiments (0.05–1.0 M), repulsive interactions between immobilized ssDNA created a compressive stress to bend the cantilever downwards. Change in surface stress with respect to change in cantilever deflection can be obtained from Stoney's formula (12) or by using the model developed in ref. 13: $\Delta\sigma/\Delta h = Et^2/4L^2\,(1-\nu) \approx 0.375$ MJ/m^2, where $\Delta\sigma$ is change in surface stress, Δh is change in deflection, $E = 180$ GN/m^2, $t = 0.5$ μm, $L = 200$ μm, and $\nu = 0.25$ are the elastic modulus, thickness, length, and Poisson's ratio of the cantilever material, respectively.

After immobilizing the probe ssDNA, a solution containing complementary target ssDNA was injected into the fluid cell at the same PB concentration used to immobilize the probe ssDNA. Fig. 3*a* shows the deflection profiles for hybridization reactions where the probe ssDNA was 20 nt long, and the complementary target ssDNA were of four different lengths (20 nt, 15 nt, 10 nt, and 9 nt) and were chosen to be distally complementary. The cluster plot of multiple experiments (2 for 15 nt and 20 nt, 3 for 9 nt and 10 nt) for each case has been included in Fig. 3*a Inset*, which shows reasonably good repeatability (within $\pm$10–15%). On the basis of reasonably good repeatability, it is suggested that the nanomechanical signal was sufficiently sensitive to detect single-nucleotide length differences. We have also performed hybridization experiments by using 30- to 50-nt-long DNA, and the results have shown very similar trends. The observation that the cantilever bent upward in all cases suggests that hybridization relieved the compressive stress created during immobilization of thiolated probe ssDNA. To confirm that the signals were caused by hybridization, a solution of a noncomplementary target ssDNA was used and was found to produce no deflection, which eliminates the possibility of false-positive signal because of nonspecific binding. Fig. 3*b* shows the steady-state deflection signal for the hybridization reaction under different PB concentrations. An optimum PB concentration of 0.2–0.4 M was seen to produce maximum deflection.

That the cantilever deflections for both the immobilization and hybridization steps were influenced by PB concentration suggests that electrostatic repulsive forces between neighboring DNA molecules must play a role in cantilever motion. The percentage of the immobilized probe ssDNA molecules that hybridize with the complementary target strands is around 60–80% (14, 16). Because each nucleotide carries a net negative charge as a result of the presence of a phosphate group, one would expect hybridization to cause even more repulsion as a result of the presence of additional negative charge. However, the data in Fig. 3 clearly indicate that regardless of the PB concentration in the range of 0.05–1 M, hybridization always relieved stress and produced upward cantilever motion. Therefore, electrostatic or steric repulsion alone cannot explain the behavior.

It is well known that, at the ionic strengths used in our experiments (0.05–1 M), ssDNA is a highly flexible molecule with a persistence length of 0.75 nm (17), which is approximately the size of 2 nucleotides. In free solution, the configuration that each ssDNA chain adopts is the one that maximizes its entropy. When ssDNA chains are grafted onto a surface, however, intermolecular interactions influence its configuration. If the grafting density of ssDNA on the Au-coated cantilever surface is sufficiently high, each ssDNA chain will be forced to occupy a region of space smaller than its natural size because of intersegment interactions resulting from steric or electrostatic repulsion. This chain deformation reduces configurational entropy. This entropic penalty can be alleviated by adsorption onto

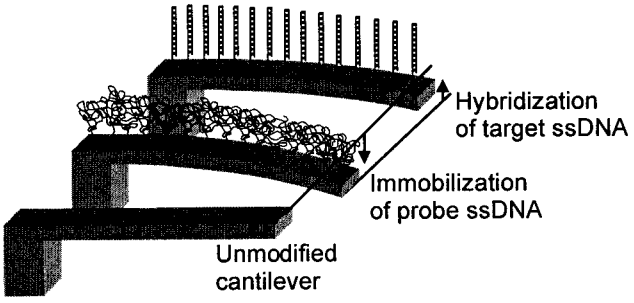

Fig. 4. Schematic diagram illustrating the mechanism of motion generation caused by DNA immobilization and hybridization. Immobilization of ssDNA on the top surface bends the cantilever down. The persistence length of ssDNA is 7.5 Å, and this flexibility provides an entropic driving force for forming curved interfaces. Hybridization increases the persistence length to about 50 nm, which significantly reduces the configurational entropic driving force, thereby reducing the importance of curvature producing an upward cantilever motion.

a convex surface, because the curvature allows each chain to occupy a larger region of space as the distance from the surface increases. This phenomenon leads to an entropic driving force in addition to the intersegment energetics for forming a curved interface. These forces are balanced by the strain energy of bending the cantilever, leading to an equilibrium value for curvature and cantilever deflection. At ionic strengths corresponding to our experiments (0.05–1 M), the persistence length of ssDNA is 0.75 nm (17), which is approximately 2 nucleotides. In contrast, the persistence length of double-stranded DNA is 50–80 nm (18), which is approximately 150 base pairs. Thus, the double-stranded DNA chains are effectively rod like, and the configurational entropy gain by forming a curved interface is insignificant compared with that of adsorbed ssDNA. Therefore, cantilever strain energy and intersegment repulsion are balanced at a smaller curvature (i.e., smaller deflection), which is illustrated schematically in Fig. 4.

A quantitative analysis corresponding to the thermodynamic arguments described above is easy to carry out for sufficiently long chains. Such an analysis would resemble that of refs. 19–21, with the added strain energy caused by cantilever bending. However, our experiments are carried out with relatively short chains. Quantitative analysis is therefore somewhat more delicate. A numerical calculation for short chains, which includes polymer conformational statistics, intersegment interactions, cantilever bending energy, and other minor effects, is currently being carried out. These computations use a discretized Greens function method (22) and should provide a quantitative description of the phenomena under consideration. Such an analysis accompanied by more extensive experimental results will be provided in a future longer account.

Experiments indicate that hybridization-induced changes in configurational entropy produce upward motion of the cantilever, leading to the question: Can the direction of cantilever motion on hybridization be reversed by controlling the change in configurational entropy? To address this question, we immobilized the probe ssDNA on the cantilever at 1.0 M PB concentration and then reduced the PB concentration to 0.1 M. Because of the higher PB concentration during immobilization, a higher packing density can be achieved because of increased shielding of the negative charges on the probe ssDNA. A subsequent reduction in PB concentration increased the Debye length, which resulted in increased repulsion between neighboring probe ssDNA. Therefore, it is favorable for the ssDNA to further stretch to reduce intermolecular repulsive energy even at the cost of reducing configurational entropy. In effect, the ssDNA

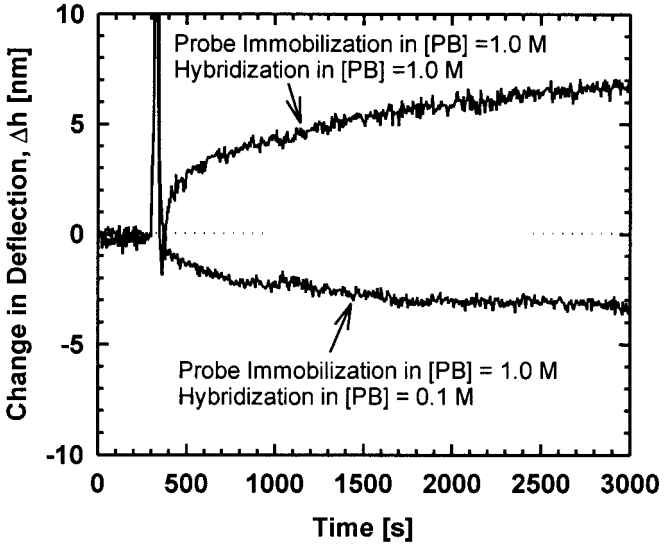

Fig. 5. Hybridization induced changes in cantilever deflection under two conditions. The 30-nt-long probe ssDNA were immobilized at 1 M PB concentration. In one case, hybridization occurred at 1 M PB concentration, which led to upward cantilever motion. In the second case, the PB concentration was first reduced to 0.1 M, after which hybridization occurred. In this case, the cantilever deflection was downward.

molecules are expected to adopt a strongly stretched configurations. Hybridization at low PB concentration should therefore lead to relatively small changes in configurational entropy. Thus, one expects the configurational entropic driving force for upward cantilever motion to play a smaller role. Because hybridization introduces additional charge, intersegment repulsive interactions are expected to increase. These arguments suggest that on hybridization under these conditions, a net downward deflection of the cantilever would be produced—exactly what we observed (see Fig. 5), which further supports our hypothesis. Also shown in Fig. 5, for comparison, are the data for immobilization and hybridization at a PB concentration at 1.0 M, where the cantilever deflection is in the upward direction. Our exper-

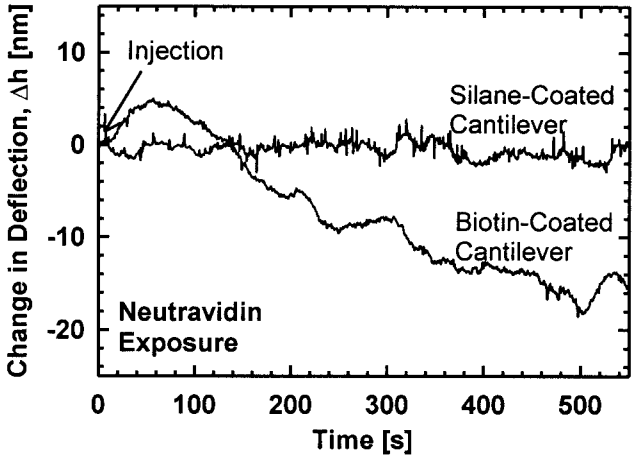

Fig. 6. Change in cantilever deflection on exposure to neutravidin. In one case, the silicon nitride surface of the cantilever was coated with biotin and polyethylene glycol, whereas in the other case, the same surface cantilever was coated with a silane layer. Specific binding of neutravidin to biotin generated a negative deflection, indicating generation of compressive stress on the top silicon nitride surface, whereas exposure to silane produced no appreciable deflection signal.

iments demonstrate that configurational entropy changes and intermolecular interactions can be tuned to control the direction of motion in nanomechanical devices.

These thermodynamic arguments suggest that nanomechanical motion would not be limited to only DNA hybridization reactions but could occur for any specific biomolecular binding—DNA–RNA, antigen–antibody (10, 11), protein–ligand, DNA–protein, etc. As a model system, we focused on the biotin–avidin complex. Experiments (23) on forced unbinding of biotin–avidin pairs have shown that the adhesive force depends linearly on the enthalpy of the reaction and is uncorrelated with the Gibbs free energy. This observation implies that the unbinding process involves no configurational entropy changes, thus suggesting that the unbinding force is purely conservative and reversible. Therefore, one would expect that because of the absence of configurational entropy changes, biotin–avidin binding on a cantilever surface would produce only repulsive intermolecular forces, which would bend a cantilever down. Fig. 6 shows the deflection profile for the biotin–neutravidin reaction, where biotin was immobilized on the silicon nitride surface of the Au/SiN_x cantilever, and neutravidin was then introduced in the fluid cell. The cantilever, with the silicon nitride surface at the top, displayed a steady downward deflection, as expected. When a silane-only cantilever was exposed to neutravidin, there was no change in the average cantilever deflection, indicating specificity in the biotin–neutravidin reaction.

In summary, we have outlined some general thermodynamic principles of how multiple biomolecular reactions can be controlled and manipulated to produce nanomechanical motion. These principles can now be used to design biomechanical actuators, switches, or motors, which could have wide use in nanotechnology. Likewise, micro- and nanomechanical devices can also be designed for studying the thermodynamics of specific biomolecular reactions. Finally, the ability to mechanically detect biomolecules offers the promising prospects of developing micromechanical arrays for high-throughput genomics and proteomics.

G.W. and A.M. thank the Engineering Program of the Department of Energy Basic Energy Sciences (Grant DE-FG03–98ER14870) and the Innovative Technologies Program of the National Cancer Institute (National Institutes of Health) (Grant R21 CA86132) for their support. K.H., H.J., and T.T. were supported by the Office of Biological and Environmental Research, the Department of Energy, under contract DE-AC05–96OR22464 with Oak Ridge National Laboratory managed by Lockheed Martin Energy Research Corporation.

1. Rastogi, V. K. & Girvin, M. E. (1991) *Nature (London)* **402,** 263–268.
2. Vale, R. D. & Milligan, R. A. (2000) *Science* **288,** 88–95.
3. Mahadevan, L. & Matsudaira, P. (2000) *Science* **288,** 95–99.
4. Astumian, R. D. & Bier, M. (1994) *Phys. Rev. Lett.* **72,** 1766–1769.
5. Astumian, R. D. (1997) *Science* **276,** 917–922.
6. Keller, D. & Bustamante, C. (2000) *Biophys. J.* **78,** 541–556.
7. Kuo, S. C. & Sheetz, M. P. (1993) *Science* **260,** 32–34.
8. Svoboda, K., Schmidt, C. F., Schnapp, B. J. & Block, S. M. (1993) *Nature (London)* **365,** 721–727.
9. Finer, J. T., Simmons, R. B. & Spuldich, J. A. (1994) *Nature (London)* **368,** 113–119.
10. Raiteri, R., Nelles, G., Butt, H.-J., Knoll, W. & Skladal, P. (1999) *Sensors Actuators B* **61,** 213–217.
11. Fritz, J., Baller, M., Lang, H. P., Rothuizen, H., Vettiger, P., Meyer, E., Güntherodt, H.-J., Gerber, Ch. & Gimzewski, J. K. (2000) *Science* **288,** 316–318.
12. Stoney, G. G. (1909) *Proc. R. Soc. London Ser. A* **82,** 172.
13. Miyatani, T. & Fujihira, M. (1997) *J. Appl. Phys.* **81,** 7099–7115.
14. Levicky, R., Herne, T. M., Tarlov, M. J. & Satija, S. K. (1998) *J. Am. Chem. Soc.* **120,** 9787–9792.
15. Georgiadis, R., Peterlinz, K. P. & Peterson, A. W. (2000) *J. Am. Chem. Soc.* **122,** 3166–3173.
16. Peterlinz, K. A. & Georgiadism R. M. (1998) *J. Am. Chem. Soc.* **119,** 3401–3402.
17. Smith, S. B., Cui, Y. & Bustamante, C. (1996) *Science* **271,** 795–799.
18. Baumann, C. G., Smith, S. B., Bloomfield, V. A. & Bustamante, C. (1997) *Proc. Natl. Acad. Sci. USA* **94,** 6185–6190.
19. Patel, S. S. & Tirrel, M. (1989) *Annu. Rev. Phys. Chem.* **40,** 587–635.
20. Wijmans, C. M. & Zhulina, E. B. (1993) *Macromolecules* **26,** 7214–7224.
21. Dan, N. & Tirrell, M. (1993) *Macromolecules* **26,** 4310–4315.
22. Fleer, G. J., Cohen Stuart, M. A., Scheutjens, J. M. H. M., Cosgrove, T. & Vincent, B. (1993) *Polymers at Interfaces* (Chapman & Hall, London).
23. Moy, V. T., Florin, E.-L. & Gaub, H. E. (1994) *Science* **266,** 257–259.